

Six networks on a universal neuromorphic computing substrate

Thomas Pfeil^{*†1} Andreas Grübl^{†1} Sebastian Jeltsch^{†1} Eric Müller^{†1}
Paul Müller^{†1} Mihai Petrovici^{†1} Michael Schmuker^{†2,3} Daniel Brüderle¹
Johannes Schemmel¹ Karlheinz Meier¹

May 29, 2022

¹Kirchhoff-Institute for Physics
Universität Heidelberg
Heidelberg, Germany

²Neuroinformatics & Theoretical Neuroscience
Freie Universität Berlin
Berlin, Germany

³Bernstein Center for Computational Neuroscience Berlin
Berlin, Germany

* Correspondence: Thomas Pfeil
Universität Heidelberg
Kirchhoff-Institute for Physics
Im Neuenheimer Feld 227
69120 Heidelberg, Germany
tel: +49-6221-549813
thomas.pfeil@kip.uni-heidelberg.de

[†] These authors contributed equally to this work. See acknowledgements for details.

Abstract

In this study, we present a highly configurable neuromorphic computing substrate and use it for emulating several types of neural networks. At the heart of this system lies a mixed-signal chip, with analog implementations of neurons and synapses and digital transmission of action potentials. Major advantages of this emulation device, which has been explicitly designed as a universal neural network emulator, are its inherent parallelism, a high speed-up factor and low power consumption compared to conventional computers. Its configurability allows the realization of almost arbitrary network topologies and the use of widely varied neuronal and synaptic parameters. Fixed-pattern noise inherent to analog circuitry is reduced by calibration routines. An integrated development environment allows neuroscientists to operate the device without any prior knowledge of neuromorphic circuit design. As a showcase for the capabilities of the system, we describe the successful emulation of six different neural networks which cover a broad spectrum of both structure and functionality.

Keywords: accelerated neuromorphic hardware system, universal computing substrate, highly configurable, mixed-signal VLSI, spiking neural networks, winner-take-all, classifier, cortical model.

1. INTRODUCTION

By nature, computational neuroscience has a high demand for powerful and efficient devices for simulating neural network models. In contrast to conventional general-purpose machines based on a von-Neumann architecture, neuromorphic systems are, in a rather broad definition, a class of devices which implement particular features of biological neural networks in their physical circuit layout (Mead, 1989; Indiveri et al., 2009; Renaud et al., 2010). In order to discern more easily between computational substrates, the term *emulation* is generally used when referring to neural networks running on a neuromorphic back-end.

Several aspects motivate the neuromorphic approach. Particularly notable, in this context, are emulation speed and power efficiency. The former is enabled by the arguably most characteristic feature of neuromorphic devices: due to the fact that individual neural network components (essentially neurons and synapses) are physically implemented *in silico*, parallelism is inherent. Due to this parallelism, scaling of emulated network models does not imply slowdown, as is usually the case for conventional machines. The hard upper bound in network size (given by the number of available components on the neuromorphic device) can be broken by scaling of the devices themselves, e.g., by wafer-scale integration (Schemmel et al., 2010) or massively interconnected chips (Merolla et al., 2011). Furthermore, dedicated circuits mimicking neural properties, either digital (Merolla et al., 2011) or mixed-signal (Indiveri et al., 2006; Brüderle et al., 2011), reduce power consumption compared to conventional computing architectures. Emulations can be further accelerated by scaling down time constants compared to biology, which is enabled by deep submicron technology (Schemmel et al., 2006, 2010; Brüderle et al., 2011).

However, in contrast to the unlimited model flexibility offered by conventional simulation, the network topology and parameter space of neuromorphic systems are often dedicated for predefined applications and therefore rather restricted (e.g., Serrano-Gotarredona et al., 2006; Merolla & Boahen, 2006; Akay, 2007; Chicca et al., 2007). Enlarging the configuration space always comes at the cost of hardware resources by occupying additional chip area and increasing power consumption. Consequently, the maximum network size is reduced, or the configurability of one aspect is decreased by increasing the configurability of another. Still, configurability costs can be counterbalanced by decreasing precision. This could concern the size of integration time steps (Merolla et al., 2011), the granularity of particular parameters (Pfeil et al., 2012) or fixed-pattern noise affecting various network components (Neftci & Indiveri, 2010; Brüderle et al., 2011). At least the latter can be, to some extent, moderated through

elaborate calibration methods (Neftci & Indiveri, 2010; Brüderle et al., 2011).

Although many research groups already provide easy access to their hardware systems (Chicca et al., 2007; Brüderle & Müller et al., 2009), limited configurability discourages a broader neuroscientific community from exploiting neuromorphic hardware systems. In this study, we present a user-friendly integrated development environment that can serve as a universal neuromorphic substrate for emulating different types of neural networks. Apart from almost arbitrary network topologies, this system provides a vast configuration space for neuron and synapse parameters (Schemmel et al., 2006; Brüderle et al., 2011). While some models can easily be transferred from software simulations to the neuromorphic substrate, others need modifications. These modifications take into account the limited hardware resources and compensate for fixed-pattern noise (Kaplan et al., 2009; Brüderle & Müller et al., 2009; Brüderle et al., 2010, 2011; Bill et al., 2010). In the following, we show six more networks emulated on our hardware system, each requiring its own hardware configuration in terms of network topology and neuronal as well as synaptic parameters.

2. THE NEUROMORPHIC SYSTEM

The central component of our neuromorphic hardware system is the neuromorphic microchip *Spikey*. It contains analog *very-large-scale integration* (VLSI) circuits modeling the electrical behavior of neurons and synapses (Figure 1). In such a *physical model*, measurable quantities in the neuromorphic circuitry have corresponding biological equivalents. For example, the membrane potential V_m of a neuron is modeled by the voltage over a capacitor C_m that, in turn, can be seen as a model of the capacitance of the cell membrane. In contrast to numerical approaches, dynamics of physical quantities like V_m evolve continuously in time. Time constants in our system are approximately 10^4 times faster than their biological counterparts. To avoid confusion between hardware and biological domains of time, voltages and currents, all parameters are specified in biological domains throughout this study.

2.1. THE NEUROMORPHIC CHIP

On *Spikey* (Figure 1), a VLSI version of the standard leaky integrate-and-fire (LIF) neuron model with conductance-based synapses is implemented (Dayan & Abbott, 2001):

$$C_m \frac{dV_m}{dt} = g_l(V_m - E_l) + \sum_i g_i(V_m - E_i) \quad (1)$$

For its hardware implementation see Figure 1 and Schemmel et al. (2006).

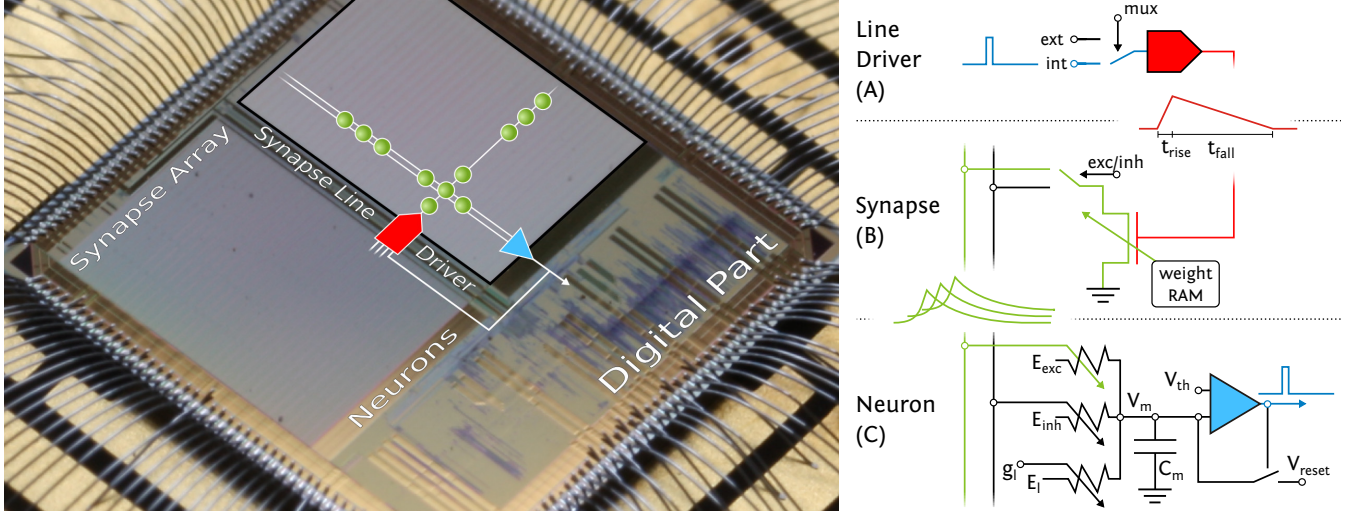


FIGURE 1: Microphotograph of the *Spikey* chip (fabricated in a 180 nm CMOS process with die size $5 \times 5 \text{ mm}^2$). Each of its 384 neurons can be arbitrarily connected to any other neuron. In the following, we give a short overview of the technical implementation of neural networks on the *Spikey* chip. **(A)** Within the synapse array 256 synapse line drivers convert incoming digital spikes (blue) into a linear voltage ramp (red). They are individually driven by either another on-chip neuron (int), e.g., the one depicted in (C), or an external spike source (ext). **(B)** Within the synapse, depending on its individually configurable weight w_i , the linear voltage ramp (red) is then translated into a current pulse (green) with exponential onset and decay. These postsynaptic pulses are sent to the neuron via the excitatory (exc) and inhibitory (inh) input line, shared by all synapses in that array column. **(C)** Upon reaching the neuron circuit, the total current on both input lines is converted into conductances, respectively. If the membrane potential V_m crosses the firing threshold V_{th} , a digital pulse (blue) is generated, which can be recorded and fed back into the synapse array. After any spike, V_m is set to V_{reset} for a refractory time period of τ_{refrac} . Neuron and synapse line driver parameters can be configured as summarized in Table 1.

Synaptic conductances g_i (with the index i running over all synapses) drive the membrane potential V_m towards the reversal potential E_i , with $E_i \in \{E_{exc}, E_{inh}\}$. The time course of the synaptic activation is modeled by

$$g_i(t) = p_i(t) \cdot w_i \cdot g_i^{\max} \quad (2)$$

where g_i^{\max} are the maximum conductances and w_i the weights for each synapse, respectively.

The implementation of spike-timing dependent plasticity (STDP; Bi & Poo, 1998; Song et al., 2000) modulating w_i over time is described in Schemmel et al. (2006) and Pfeil et al. (2012). Correlation measurement between pre- and post-synaptic action potentials is carried out in each synapse, and the 4-bit weight is updated by an on-chip controller located in the digital part of the *Spikey* chip. However, STDP will not be further discussed in this study.

Short-term plasticity (STP) modulates g_i^{\max} (Schemmel et al., 2007) similar to the model by Tsodyks & Markram (1997) and Markram et al. (1998). On hardware, STP can be configured individually for each synapse line driver that corresponds to an axonal connection in biological terms. It can either be facilitating or depressing.

The propagation of spikes within the *Spikey* chip is illustrated in Figure 1. *Spikes* enter the chip as time-stamped events using standard digital signaling techniques that facilitate long-range communication, e.g., to the host computer or other chips. Such digital packets are processed in discrete time in the digital part of the chip, where they are transformed into digital *pulses* entering the synapse line driver (blue in Figure 1A). These pulses propagate in continuous time between on-chip neurons, and are optionally transformed back into digital spike packets for off-chip communication.

2.2. SYSTEM ENVIRONMENT

The *Spikey* chip is mounted on a network module schematized in Figure 2 and described in Fieres et al. (2004). Digital spike and configuration data is transferred via direct connections between a field-programmable gate array (FPGA) and the *Spikey* chip. Onboard digital-to-analog converter (DAC) and analog-to-digital converter (ADC) components supply external parameter voltages to the *Spikey* chip and digitize selected voltages generated by the chip for calibration purposes. Furthermore, up to eight selected membrane voltages can be recorded in parallel by an oscilloscope. Because communication

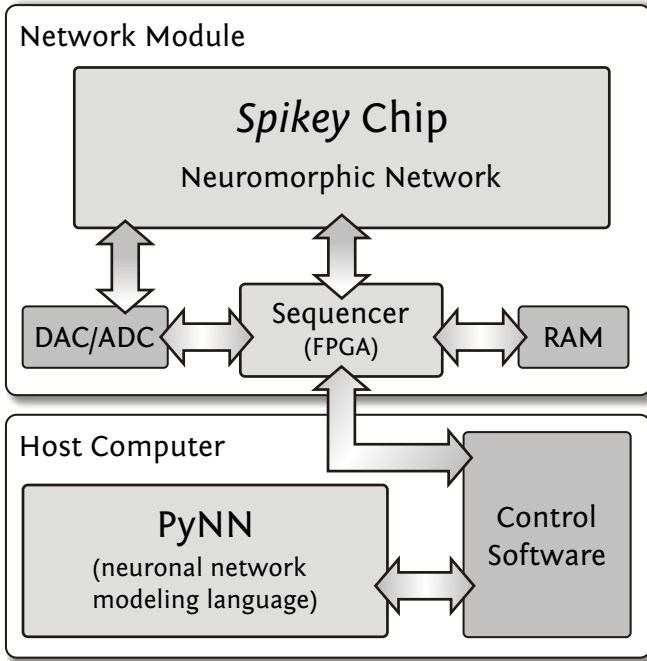


FIGURE 2: Integrated development environment: User access to the *Spikey* chip is provided using the PyNN neural network modeling language. The control software controls and interacts with the network module which is operating the *Spikey* chip.

between a host computer and the FPGA has a limited bandwidth that does not satisfy real-time operation requirements of the *Spikey* chip, experiment execution is controlled by the FPGA while operating the *Spikey* chip in continuous time. To this end, all experiment data is stored in the local random access memory (RAM) of the network module.

Execution of an experiment is split up into three steps (Figure 2). First, the *control software* within the memory of the host computer generates configuration data (Table 1, e.g., synaptic weights, network connectivity, etc.), as well as input stimuli to the network. All data is stored as a sequence of commands and is transferred to the memory on the network module. In the second step, a playback sequencer in the FPGA logic interprets this data and sends it to the *Spikey* chip, as well as triggers the emulation. Data produced by the chip, e.g., neuronal activity in terms of spike times, is recorded in parallel. In the third and final step, this recorded data stored in the memory on the network module are retrieved and transmitted to the host computer, where they are processed by the control software.

Having a control software that abstracts hardware greatly simplifies modeling on the neuromorphic hardware system. However, modelers are already struggling with multiple incompatible interfaces to software simu-

lators. That is why our neuromorphic hardware system supports PyNN, a widely used application programming interface (API) that strives for a coherent user interface, allowing portability of neural network models between different software simulation frameworks (e.g., NEST or NEURON) and hardware systems (e.g., the *Spikey* system). For details see Gewaltig & Diesmann (2007); Eppler et al. (2009) for NEST, Carnevale & Hines (2006); Hines et al. (2009) for NEURON, Brüderle et al. (2011); Brüderle & Müller et al. (2009) for the *Spikey* chip, and Davison et al. (2009, 2010) for PyNN, respectively.

2.3. CONFIGURABILITY

In order to facilitate the emulation of network models inspired by biological neural structures, it is essential to support the implementation of different (cortical) neuron types. From a mathematical perspective, this can be achieved by varying the appropriate parameters of the implemented neuron model (Equation 1).

To this end, the *Spikey* chip provides 2969 different analog parameters (Table 1) stored on current memory cells that are continuously refreshed from a digital on-chip memory. Most of these cells deliver individual parameters for each neuron (or synapse line driver), e.g., leakage conductances g_l . Due to the size of the current-voltage conversion circuitry it was not possible to provide individual voltage parameters, such as, e.g., E_l , E_{exc} and E_{inh} , for each neuron. As a consequence, groups of 96 neurons share most of these voltage parameters. Parameters that can not be controlled individually are delivered by global current memory cells.

In addition to the possibility of controlling analog parameters, the *Spikey* chip also offers an almost arbitrary configurability of the network topology. As illustrated in Figure 1, the fully configurable *synapse array* allows connections from synapse line drivers (located alongside the array) to arbitrary neurons (located below the array) via synapses whose weights can be set individually with a 4-bit resolution. This limits the maximum input count to 256 synapses per neuron, up to 192 synapses from on-chip neurons and up to 256 from external spike sources.

2.4. CALIBRATION

Device mismatch that arises from hardware production variability causes fixed-pattern noise, which causes parameters to vary from neuron to neuron as well as from synapse to synapse. Electronic noise (including thermal noise) also affects dynamic variables, as, e.g., the membrane potential V_m . Consequently, experiments will exhibit some amount of both neuron-to-neuron and trial-to-trial variability given the same input stimulus. It is, however, important to note that these types of variations are not unlike the neuron diversity and response stochas-

Scope	Name	Type	Description
Neuron circuits (A)	n/a	i _n	Two digital configuration bits activating the neuron and readout of its membrane voltage
	g_l	i _n	Bias current for neuron leakage circuit
	τ_{refrac}	i _n	Bias current controlling neuron refractory time
	E_l	s _n	Leakage reversal potential
	E_{inh}	s _n	Inhibitory reversal potential
	E_{exc}	s _n	Excitatory reversal potential
	V_{th}	s _n	Firing threshold voltage
Synapse line drivers (B)	V_{reset}	s _n	Reset potential
	n/a	i _l	Two digital configuration bits selecting input of line driver
	n/a	i _l	Two digital configuration bits setting line excitatory or inhibitory
	$t_{\text{rise}}, t_{\text{fall}}$	i _l	Two bias currents for rising and falling slew rate of presynaptic voltage ramp
Synapses (B)	g_i^{max}	i _l	Bias current controlling maximum voltage of presynaptic voltage ramp
	w	i _s	4-bit weight of each individual synapse
STP related (C)	n/a	i _l	Two digital configuration bits selecting short-term depression or facilitation
	U_{SE}	i _l	Two digital configuration bits tuning synaptic efficacy for STP
	n/a	s _l	Bias voltage controlling spike driver pulse length
	$\tau_{\text{rec}}, \tau_{\text{facil}}$	s _l	Voltage controlling STP time constant
	I	s _l	Short-term facilitation reference voltage
STDP related (D)	R	s _l	Short-term capacitor high potential
	n/a	i _l	Bias current controlling delay for presynaptic correlation pulse (for calibration purposes)
	$A_{+/-}$	s _l	Two voltages dimensioning charge accumulation per (anti-)causal correlation measurement
	n/a	s _l	Two threshold voltages for detection of relevant (anti-)causal correlation
	τ_{STDP}	g	Voltage controlling STDP time constants

TABLE 1: List of analog current and voltage parameters as well as digital configuration bits. Each with corresponding model parameter names, excluding technical parameters that are only relevant for correctly biasing analog support circuitry or controlling digital chip functionality. Electronic parameters that have no direct translation to model parameters are denoted *n/a*. The membrane capacitance is fixed and identical for all neuron circuits ($C_m = 0.2 \text{ nF}$ in biological value domain). Parameter types: (i) controllable for each corresponding circuit: 192 for neuron circuits (denoted with subscript *n*), 256 for synapse line drivers (denoted with subscript *l*), 49152 for synapses (denoted with subscript *s*), (s) two values, shared for all even/odd neuron circuits or synapse line drivers, respectively, (g) global, one value for all corresponding circuits on the chip. All numbers refer to circuits associated to one synapse array and are doubled for the whole chip. For technical reasons, the current revision of the chip only allows usage of one synapse array of the chip. Therefore, all experiments presented in this paper are limited to a maximum of 192 neurons. For parameters denoted by (A) see Equation 1 and Schemmel et al. (2006), for (B) see Figure 1, Equation 2 and Dayan & Abbott (2001), for (C) see Schemmel et al. (2007) and for (D) see Schemmel et al. (2006) and Pfeil et al. (2012).

ticity found in biology (Gupta et al., 2000; Maass et al., 2002; Marder & Goaillard, 2006; Rolls & Deco, 2010).

To facilitate modeling and provide repeatability of experiments on arbitrary *Spikey* chips, it is essential to minimize these effects by calibration routines. Many calibrations have directly corresponding biological model parameters, e.g., membrane time constants (described in the following), firing thresholds, synaptic efficacies or PSP shapes. Others have no equivalents, like compensations for shared parameters or workarounds of defects (e.g., Kaplan et al., 2009; Bill et al., 2010; Pfeil et al., 2012). In general, calibration results are used to improve the mapping between biological input parameters and the corresponding target hardware voltages and currents, as well

as to determine the dynamic range of all model parameters (e.g., Brüderle & Müller et al., 2009).

While the calibration of most parameters is rather technical, but straightforward (e.g., all neuron voltage parameters), some require more elaborate techniques. These include the calibration of τ_m , STP as well as synapse line drivers, as we describe later for individual network models. The membrane time constant $\tau_m = C_m/g_l$ differs from neuron to neuron mostly due to variations in the leakage conductance g_l . However, g_l is independently adjustable for every neuron. Because this conductance is not directly measurable, an indirect calibration method is employed. To this end, the threshold potential is set below the resting potential. Following each spike, the membrane potential is clamped to V_{reset} for an absolute

refractory time τ_{refrac} , after which it evolves exponentially towards the resting potential E_l until the threshold voltage triggers a spike and the next cycle begins. If the threshold voltage is set to $V_{\text{th}} = E_l - 1/e \cdot (E_l - V_{\text{reset}})$, the spike frequency equals $1/(\tau_m + \tau_{\text{refrac}})$, thereby allowing an indirect measurement and calibration of E_l and therefore τ_m . For a given τ_m and $\tau_{\text{refrac}} = \text{const}$, V_{th} can be calculated. An iterative method is applied to find the best-matching V_{th} , because the exact hardware values for E_l , V_{reset} and V_{th} are only known after the measurement. The effect of calibration on a typical chip can best be exemplified for a typical target value of $\tau_m = 10$ ms. Before calibration, τ_m values are randomly distributed, with mean and standard deviation $(\mu, \sigma) = (17.5 \text{ ms}, 12.8 \text{ ms})$. After calibration, the distribution mean lies very close to the target value and the variance drops significantly: $(\mu, \sigma) = (10.9 \text{ ms}, 1.9 \text{ ms})$.

The STP hardware parameters have no direct translation to model equivalents. In fact, the implemented transconductance amplifier tends to easily saturate within the available hardware parameter ranges. These non-linear saturation effects can be hard to handle in an automated fashion on an individual circuit basis. Consequently, the translation of these parameters is based on STP courses averaged over several circuits.

3. HARDWARE EMULATION OF NEURAL NETWORKS

In the following, we present six neural network models that have been emulated on the *Spikey* chip. Most of the emulation results are compared to those obtained by software simulations in order to verify the network functionality and performance. For all these simulations the tool NEST (Gewaltig & Diesmann, 2007) or NEURON (Carnevale & Hines, 2006) is used.

3.1. SYNFIRE CHAIN WITH FEEDFORWARD INHIBITION

Architectures with a feedforward connectivity have been employed extensively as computational components and as models for the study of neuronal dynamics. Synfire chains are feedforward networks consisting of several neuron groups where each neuron in a group projects to neurons in the succeeding group.

They have been originally proposed to account for the presence of behaviorally-related, highly precise firing patterns (Baker et al., 2001; Prut et al., 1998). Further properties of such structures have been studied extensively, including activity transport (Aertsen et al., 1996; Diesmann et al., 1999; Litvak et al., 2003), external control of information flow (Kremkow et al., 2010), computational capabilities (Abeles et al., 2004; Vogels & Abbott, 2005; Schrader et al., 2010), complex dynamic behavior (Yazdanbakhsh et al., 2002) and their embedding into sur-

rounding networks (Aviel et al., 2003; Tetzlaff et al., 2005; Schrader et al., 2008). Kremkow et al. (2010) have shown that feedforward inhibition can increase the selectivity to the initial stimulus and that the local delay of inhibition can modify this selectivity.

3.1.1. Network Topology

The presented network model is an adaptation of the *feedforward network* described in Kremkow et al. (2010).

The network consists of several neuron groups, each comprising n_{RS} excitatory regular spiking (RS) and n_{FS} inhibitory fast spiking (FS) cells. All neurons are modeled as LIF neurons with exponentially decaying synaptic conductance courses. According to Kremkow et al. (2010) all neurons have identical parameters.

As shown in Figure 3A, RS neurons project to both RS and FS populations in the subsequent group while the FS population projects to the RS population in its local group. Each neuron receives a fixed number of randomly chosen inputs from each presynaptic population. The first group is stimulated by a population of n_{RS} external spike sources with identical connection probabilities as used for RS groups within the chain.

Two different criteria are employed to assess the functionality of the emulated synfire chain. The first, straightforward benchmark is the stability of signal propagation. An initial synchronous stimulus is expected to cause a stable propagation of activity, with each neuron in an RS population spiking exactly once. Deviations from the original network parameters can cause the activity to grow rapidly, i.e., each population emits more spikes than its predecessor, or stall pulse propagation.

The second, broader characterization follows Kremkow et al. (2010), who has analyzed the response of the network to various stimuli. The stimulus is parametrized by the variables a and σ . For each neuron in the stimulus population a spike times are generated by sampling them from a Gaussian distribution with common mean and standard deviation. σ is defined as the standard deviation of the spike times of all source neurons. Spiking activity that is evoked in the subsequent RS populations is characterized analogously by measuring a and σ .

Figure 3C shows the result of a software simulation of the original network. The filter properties of the network are reflected by a separatrix dividing the state space shown in Figure 3C and D into two areas, each with a different fixed point. First, the basin of attraction (dominated by red circles in Figure 3C) from which stable propagation can be evoked and second, the remaining region (dominated by crosses in Figure 3C) where any initial activity becomes extinguished. This separatrix determines which types of initial input lead to a stable signal propagation.

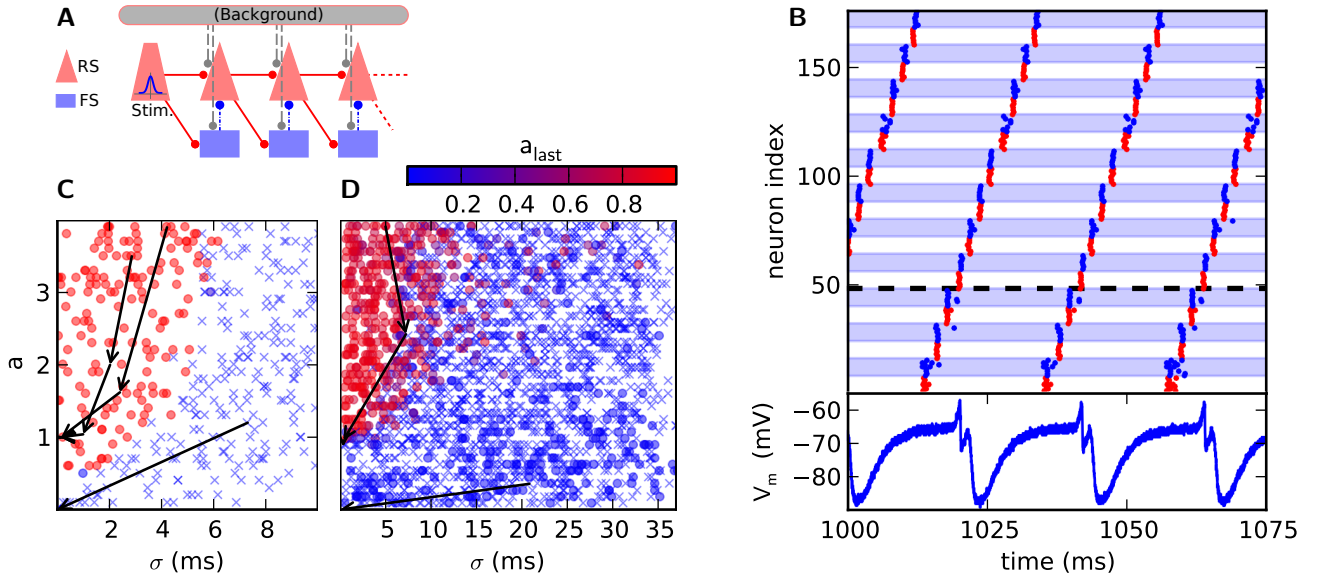


FIGURE 3: (A) Synfire chain with feedforward inhibition. The background is only utilized in the original model, where it is implemented as random Gaussian current. For the presented hardware implementation it has been omitted due to network size constraints. As compensation for missing background stimuli, the resting potential was increased to ensure a comparable excitability of the neurons. **(B)** Hardware emulation. Top: Raster plot of pulse packet propagation 1000 ms after initial stimulus. Spikes from RS groups are shown in red and spikes from FS groups are denoted by blue color and background. Bottom: Membrane potential of the first neuron in the fourth RS group, which is denoted by a dashed horizontal line. The cycle duration is approximately 20 ms. **(C)** State space generated with software simulations of the original model. The position of each marker indicates the (σ, a) parameters of the stimulus while the color encodes the activity in the RS population of the third synfire group. Lack of activity is indicated with a cross. The evolution of the pulse packet parameters is shown for three selected cases by a series of arrows. Activity either stably propagates with fixed point $(\sigma, a) = (0.1 \text{ ms}, 1)$ or extinguishes with fixed point $(\sigma, a) = (0 \text{ ms}, 0)$. **(D)** Same as (C), but emulated on the FACETS chip-based system. The fixed point of stable propagation is located at $(\sigma, a) = (0.3 \text{ ms}, 1)$.

3.1.2. Hardware Emulation

The size and parameter constraints of the hardware did not allow to achieve both benchmark requirements of stable pulse propagation and input selectivity with a single network implementation. Consequently, two different versions were realized, with different number and size of neuron populations.

To demonstrate a stable propagation of pulses, a large number of consecutive group activations was needed. The chain was configured as a loop by connecting the last group to the first, allowing the observation of more pulse packet propagations than there are groups in the network. Synaptic delays are determined by the speed of signal propagation on the *Spikey* chip and are hence fixed to approximately 1 ms. In conjunction with the limited number of available neurons this caused pulse packets to pass the cycle frequently. On the other hand, this frequency had to be small enough to allow the spiking neurons to recover from the previous activation. Consequently, the frequency was minimized by maximizing the number of groups. This decreased population sizes which, in turn,

affected the stability of propagation. The original ratio of 20% inhibitory FS cells could not be maintained for the reduced population size as inhibition would be too weak and unreliable to stabilize activity propagation. We have found $n_{RS} = n_{FS} = 8$ to provide a satisfactory trade-off.

To further improve propagation properties, the membrane time constant was lowered for all neurons by raising g_l to its maximum value. The strength of inhibition was increased by setting the inhibitory synaptic weight to its maximum value and lowering the inhibitory reversal potential to its minimum value. Finally, the synaptic weights $RS_i \rightarrow RS_{i+1}$ and $RS_i \rightarrow FS_{i+1}$ were adjusted. These improvements resulted in synfire propagation being stable for at least 2 h wall-clock time which corresponds to more than 2 years in biological real-time.

The second network demonstrates the filtering properties of a hardware-emulated synfire chain with feedforward inhibition. This use case required larger synfire groups than in the first case as otherwise, the total excitatory conductance caused by a pulse packet with large σ was usually not smooth enough due to the low number of spikes. Thus, three groups were placed on a single chip

with $n_{RS} = 45$ and $n_{FS} = 18$. The resulting evolution of pulse packets is shown in Figure 3D. After passing three groups, most runs resulted in either very low activity in the last group or were located near the fixed point of stable propagation. The separation in the parameter space of the initial stimulus is not as sharply bounded as in the case of the original network (Figure 3C). Nevertheless, the filtering properties of the network are apparent. The filtering quality could be improved by employing the original group size, which would require using a large scale neuromorphic device (see, e.g., Schemmel et al., 2010).

Our hardware implementation of the synfire chain model demonstrates the possibility to run extremely long lasting experiments due to the high speed-up factor of the hardware system. Because the synfire chain model itself does not require sustained external stimulus, it could be employed as an autonomous source of periodic input to other experiments.

3.2. BALANCED RANDOM NETWORK

Brunel (2000) reports *balanced random networks* (BRNs) exhibiting, among others, asynchronous irregular network states with stationary global activity.

3.2.1. Network Topology

BRNs consist of an inhibitory and excitatory population of neurons, both stimulated by two populations of Poisson processes mimicking background activity. Additionally, both neuron populations project onto themselves as well as the other. All projections are realized with random and sparse connections of probability p . In order to obtain an asynchronous irregular network state, synaptic weights for inhibitory connections are chosen four times larger than those for excitatory ones. In contrast to the original implementation using 12500 neurons, we scaled this network by a factor of 100 while preserving its firing behavior.

If single cells fire irregularly, the *coefficient of variation*

$$C_V = \frac{\sigma_T}{\bar{T}} \quad (3)$$

of interspike intervals has values close to or higher than one (Dayan & Abbott, 2001). \bar{T} and σ_T are the mean and standard deviation of these intervals. Synchrony between two cells can be measured by calculating the *correlation coefficient*

$$C_C = \frac{\text{cov}(n_1, n_2)}{\sqrt{\text{var}(n_1)\text{var}(n_2)}} \quad (4)$$

of their spike trains n_1 and n_2 , respectively (Parker et al., 1967). Here, time bins of 2 ms are used (Kumar et al., 2008).

Brüderle et al. (2010) have shown another approach to investigate networks inspired by Brunel (2000). Their focus have been the effects of network parameters and STP on the firing rate of the network.

3.2.2. Hardware Emulation

In addition to standard calibration routines (Section 2.4), we have calibrated the chip explicitly for the BRN shown in Figure 4A. In the first of two steps, excitatory and inhibitory synapse line drivers were calibrated sequentially towards equal strength, respectively, but with inhibition four times stronger than excitation. To this end, all available neurons received spiking activity from a single synapse line driver, thereby averaging out neuron-to-neuron variations. The shape of synaptic conductances (specifically t_{fall} and g_i^{max}) were adjusted to obtain a target mean firing rate of 10 Hz over all neurons. Similarly, each driver was calibrated for its inhibitory operation mode. All neurons were strongly stimulated by an additional driver with its excitatory mode already calibrated, and again the shape of conductances, this time for inhibition, was adjusted to obtain the target rate.

Untouched by this prior calibration towards a target mean rate, neuron excitability still varied between neurons and was calibrated consecutively for each neuron in a second calibration step. For this, all neurons of the BRN were used to stimulate a single neuron with a total firing rate that was uniformly distributed among all inputs and equal to the estimated firing rate of the final network implementation. Subsequently, all afferent synaptic weights to this neuron were scaled in order to adapt its firing rate to the target rate. To further stabilize the network, efferent connections of the excitatory neuron population were modeled as short-term depressing.

Figure 4B and C show recordings of a BRN emulation on a calibrated chip with neurons firing irregularly and asynchronously. Note that $C_V \geq 1$ does not necessarily guarantee an exponential interspike interval distribution and even less Poisson firing. However, neurons within the BRN clearly exhibit irregular firing (Figure 4B and D).

A simulation of the same network topology and stimulus using software tools produced similar results. Synaptic weights were not known for the hardware emulation, but defined by the target firing rates using the above calibration. A translation to biological parameters is possible, but would have required further measurements and was not of further interest in this context. Instead, for software simulations, the synaptic weight for excitatory connections were chosen to fit the mean firing rate of the hardware emulation (approx. 9 Hz). Then, the weight of inhibitory connections were chosen to preserve the ratio between inhibitory and excitatory weights.

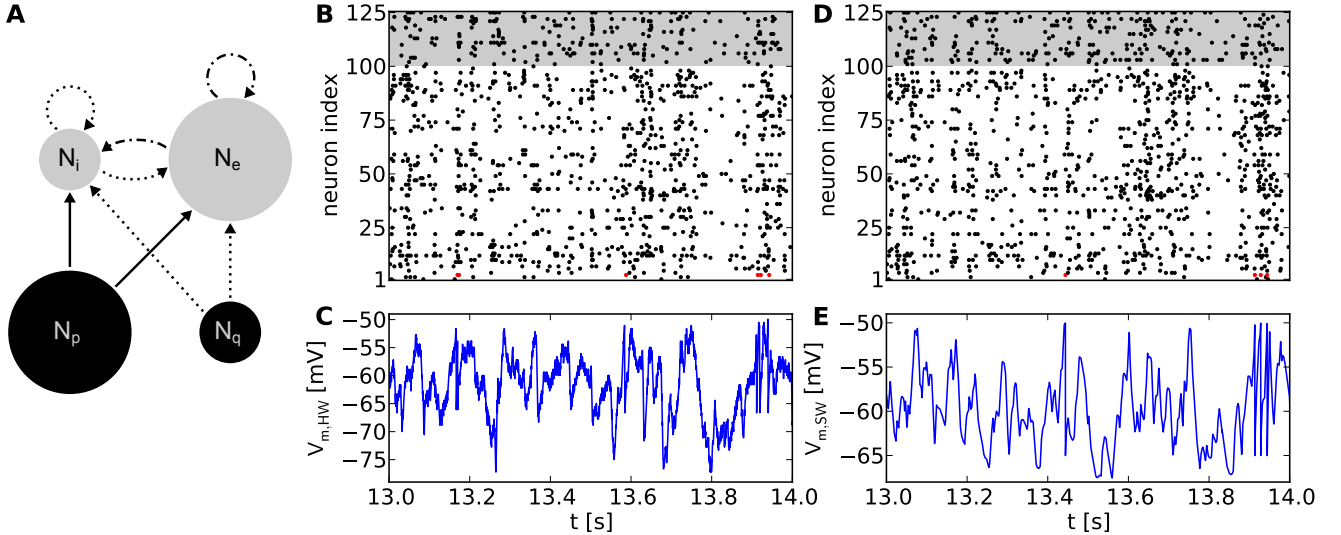


FIGURE 4: Network topology of a balanced random network. **(A)** Populations consisting of $N_e = 100$ excitatory and $N_i = 25$ inhibitory neurons (gray circles), respectively, are stimulated by populations of Poisson sources (black circles). We use $N_p = 100$ independent sources for excitation and $N_q = 25$ for inhibition. Arrows denote projections between these populations with connection probabilities $p = 0.1$, with solid lines for excitatory and dotted lines for inhibitory connections. Dot and dash lines are indicating excitatory projections with short-term depression. **(B)** Raster plot for a hardware emulation (HW) on the *Spikey* chip. Populations of excitatory and inhibitory neurons are depicted with white and gray background, respectively. Note that for clarity only the time interval [13s..14s] of a 20s emulation is shown. For the full 20s emulation, we have measured $C_V = 1.02 \pm 0.16$ (mean over all neurons) and $C_C = 0.014 \pm 0.019$ (mean over 1000 random chosen pairs of neurons), respectively. **(C)** Recorded membrane potential of an arbitrary excitatory neuron (neuron index 3, highlighted in red in the above raster plot). **(D), (E)** Same network topology and stimulus as in (B) and (C), but simulated with software (SW), resulting in $C_V = 0.96 \pm 0.09$ and $C_C = 0.010 \pm 0.017$.

Membrane dynamics of single neurons within the network are comparable between hardware emulations and software simulations (Figure 4C and E). Evidently, spike times differ between the two approaches due to various hardware noise sources (Section 2.4). However, we observe that these phenomena have no effect in large populations of neurons and result in firing statistics comparable to software simulations (compare Figure 4B and D). The ability to reproduce these statistics is highly relevant in the context of cortical models which rely on asynchronous irregular firing activity for information processing (e.g., van Vreeswijk & Sompolinsky, 1996).

3.3. WINNER-TAKE-ALL NETWORK

Winner-take-all (WTA) computation is often viewed as an underlying principle in models of cortical processing (Grossberg, 1973; Maass, 2000; Itti & Koch, 2001; Oster et al., 2009; Lundqvist et al., 2010). This is one reason for which many neuromorphic systems explicitly implement WTA architectures (Lazzaro et al., 1988; Chicca et al., 2007; Neftci & Indiveri, 2010).

3.3.1. Network Topology

We implemented a WTA network that is composed of recurrently connected excitatory and a common pool of inhibitory neurons (Figure 5A), similar to the one published by Neftci & Indiveri (2010). The ring-shaped layer of excitatory neurons is stimulated at two opposing sides with firing rates r_1 and r_2 . Depending on the contrast between input firing rates, one side of the ring wins by firing with a higher rate and thereby suppressing the other.

3.3.2. Hardware Emulation

Hardware emulations of the WTA network show comparable discrimination performance to software simulations (Figure 5B and C). Figure 5D and E depict activity profiles of the neuron layers illustrating recurrent excitation. The asymmetry in case of hardware neurons expresses the inhomogeneity of their excitability (Section 2). In case of hardware emulations, each stimulus was distributed and hence averaged over 5 synapse line drivers in order to equalize stimulation strength among neurons. For both back-ends, inhibitory weights were chosen four times stronger than excitatory ones (using the synapse line driver calibration of Section 3.2), but their absolute values differed. However, the hardware system shows

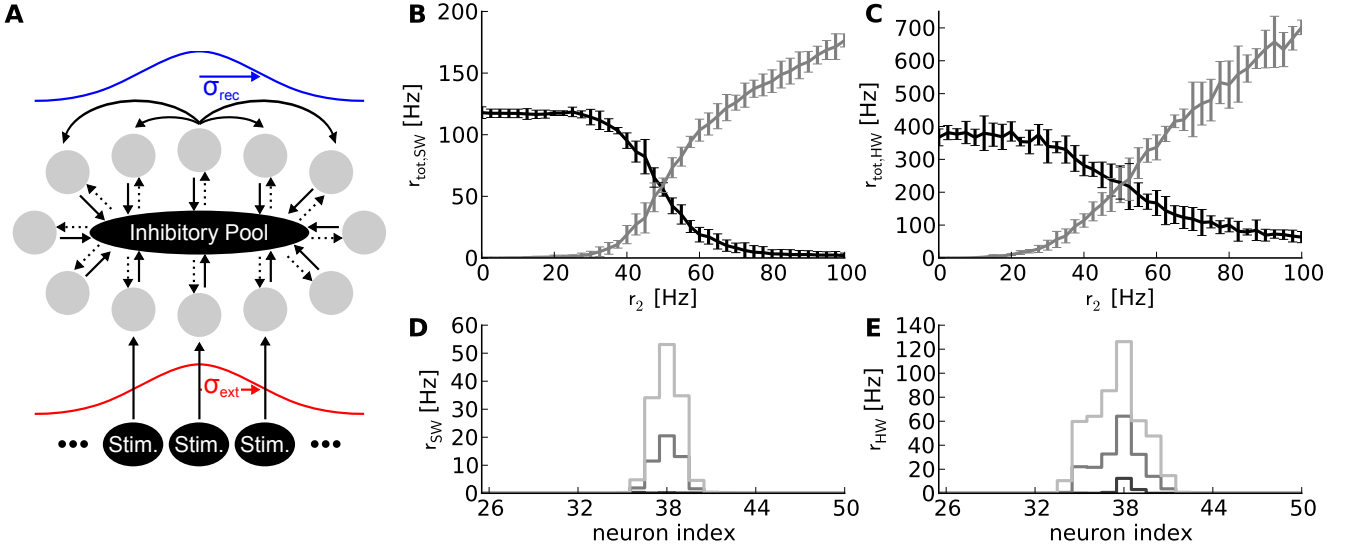


FIGURE 5: (A) Topology of a soft winner-take-all network. Recurrently connected excitatory neurons are located on a ring-shaped layer (50 neurons; gray circles), and project bidirectionally to a common inhibitory pool (16 neurons; upper black ellipse). Each of the excitatory neurons projects to its neighboring neurons with synaptic weights decreasing with distance on the ring. More precisely, synaptic weights are a function of distance following a Gaussian profile with its mean μ at the presynaptic neuron, whereas the standard deviation σ is expressed by the distance between neurons (for recurrent connections between excitatory neurons: $\sigma_{\text{rec}} = 5$ neurons; blue). Similarly, weights of external stimulation also follow a Gaussian profile with mean μ_{ext} and standard deviation $\sigma_{\text{ext}} = 3$ neurons (red). Each neuron located within a distance of $3\sigma_{\text{ext}}$ is stimulated by an external Poisson spike sources firing at 5 Hz (lower black ellipse). Solid arrows denote excitatory and dotted arrows inhibitory connections. **(B)** Software simulation (SW). One side of the ring ($\mu_{\text{ext}} = \text{neuron index } 13$; black) is stimulated with $r_1 = 50$ Hz while the firing rate r_2 of the stimulus on the other side ($\mu_{\text{ext}} = \text{neuron index } 38$; gray) is varied. The total output firing rate r_{tot} (mean over 5 runs at 2 s duration with different random numbers each) for each half of the ring is plotted against r_2 . **(C)** Same as (B), but emulated on *Spikey* (HW). **(D)** Firing rate distribution over neuron indices for $r_2 = 25$ Hz (black), 50 Hz (dark gray) and 75 Hz (light gray). **(E)** Same as (D), but emulated on *Spikey*.

more reliable performance for high weights, resulting in increased firing rates $r_{\text{tot,HW}}$. The contrast between firing rates r_{tot} at high input rates r_2 is less distinctive for hardware emulations compared to software simulations. Nevertheless, WTA functionality is well reproduced on the *Spikey* chip qualifying our hardware system for applications relying on similar WTA network topologies.

3.4. CORTICAL LAYER 2/3 ATTRACTOR MODEL

Throughout the past decades, attractor networks that model working memory in the cerebral cortex have gained increasing support from both experimental data and computer simulations. The *cortical layer 2/3 attractor memory model* described in Lundqvist et al. (2006, 2010) has been remarkably successful at reproducing both low-level (firing patterns, membrane potential dynamics) and high level (pattern completion, attentional blink) features of cortical information processing. One particularly valuable aspect is the very low amount of fine-tuning this model requires in order to reproduce the rich set of desired internal dynamics. It has also been shown in Brüderle

et al. (2011) that there are multiple ways of scaling this model down in size without affecting its main functionality features. These aspects make it an ideal candidate for implementation on our analog neuromorphic device. In this context, it becomes particularly interesting to analyze how the strong feedback loops which predominantly determine the characteristic network activity are affected by the imposed limitations of the neuromorphic substrate and fixed-pattern noise.

3.4.1. Network Topology

From a structural perspective, the most prominent feature of the Layer 2/3 Attractor Memory Network is its modularity. Faithful to its biological archetype, it implements a set of cortical hypercolumns, which are in turn subdivided into multiple minicolumns (Figure 6A). Each minicolumn consists of three cell populations: excitatory pyramidal cells, inhibitory basket cells and inhibitory RSNP (regular spiking non-pyramidal) cells.

Attractor dynamics arise from the synaptic connectivity on two levels. Within a hypercolumn, the basket cell

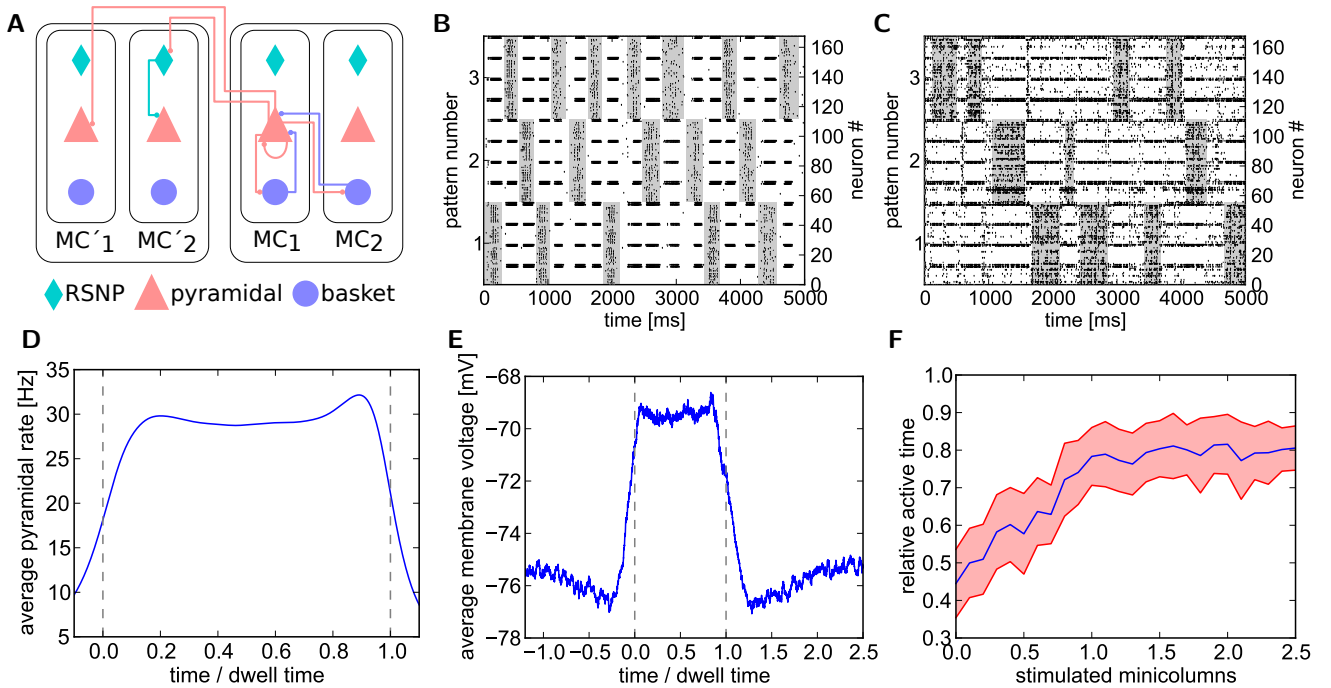


FIGURE 6: (A) Schematic of the cortical layer 2/3 attractor memory network. Two hypercolumns, each containing two minicolumns, are shown. For better readability, only connections that are active within an active pattern are depicted. See text for details. **(B)** Software simulation of spiking activity in the cortical attractor network model scaled down to 192 neurons (only pyramidal and RSNP cells shown, basket cells spike almost continuously). Minicolumns belonging to the same pattern are grouped together. The broad stripes of activity are generated by pyramidal cells in active attractors. The interlaced narrow stripes of activity represent pairs of RSNP cells, which spike when their home minicolumn is inhibited by other active patterns. **(C)** Same as **B**, but on hardware. The raster plot is noisier and the duration of attractors (dwell time) are less stable than in software due to fixed-pattern noise on neuron and synapse circuits. For better readability, active states are underlined in grey in **B** and **C**. **(D)** Average firing rate of pyramidal cells on the *Spikey* chip inside active patterns. **(E)** Average membrane potential of pyramidal cells on the *Spikey* chip inside and outside active patterns. To allow averaging over multiple active periods of varying lengths, all attractor dwell times have been normalized to 1 in **D** and **E**. **(F)** Pattern completion on the *Spikey* chip. Average values (from multiple runs) depicted in blue, with the standard deviation shown in red. From a relatively equilibrated state where all patterns take turns in being active, additional stimulation (see text) of only a subset of neurons from a given attractor activates the full pattern and enables it to dominate over the other two. The pattern does not remain active indefinitely due to short-term depression in excitatory synapses, thereby still allowing short occasional activations of the other two patterns.

population enables a soft-WTA-like competition among the pyramidal populations within the minicolumns. On a global scale, the long-range inhibition mediated by the RSNP cells governs the competition among so-called *patterns*, as explained in the following.

In the original model described in Lundqvist et al. (2010), each hypercolumn contains 9 minicolumns, each of which consists of 30 pyramidal, 2 RSNP and 1 basket cells. Within a minicolumn, the pyramidal cells are interconnected and also project onto the 8 closest basket cells within the same hypercolumn. In turn, pyramidal cells in a minicolumn receive projections from all basket cells within the same hypercolumn. All pyramidal cells receive two types of additional excitatory input: an evenly

distributed amount of diffuse Poisson noise and specific activation from the cortical layer 4. Therefore, the minicolumns (i.e., the pyramidal populations within) compete among each other in WTA-like fashion, with the winner being determined by the overall strength of the received input.

A pattern (or attractor) is defined as containing exactly one minicolumn from each hypercolumn. Considering only orthogonal patterns (each minicolumn may only belong to a single pattern) and given that all hypercolumns contain an equal amount of minicolumns, the number of patterns in the network is equal to the number of minicolumns per hypercolumn. Pyramidal cells within each minicolumn project onto the pyramidal cells

of all the other minicolumns in the same pattern. These connections ensure a spread of local activity throughout the entire pattern. Additionally, the pyramidal cells also project onto the RSNP cells of all minicolumns belonging to different attractors, which in turn inhibit the pyramidal cells within their minicolumn. This long-range competition enables the winning pattern to completely shut down the activity of all other patterns.

Two additional mechanisms weaken active patterns, thereby facilitating switches between patterns. The pyramidal cells contain an adaptation mechanism which decreases their excitability with every emitted spike. Additionally, the synapses between pyramidal cells are modeled as short-term depressing.

3.4.2. Hardware Emulation

When scaling down the original model (2673 neurons) to the maximum size available on the *Spikey* chip (192 neurons, see Figure 6B for software simulation results), we made use of the essential observation that the number of pyramidal cells can simply be reduced without compensating for it by increasing the corresponding projection probabilities. Also, for less than 8 minicolumns per hypercolumn, all basket cells within a hypercolumn have identical afferent and efferent connectivity patterns, therefore allowing to treat them as a single population. Their total number was decreased, while increasing their efferent projection probabilities accordingly. In general (i.e., except for pyramidal cells), when number and/or size of populations were changed, projection probabilities were scaled in such a way that the total fan-in for each neuron was kept at a constant average. When the maximum fan-in was reached (one afferent synapse for every neuron in the receptive field), the corresponding synaptic weights were scaled up by the remaining factor.

Because neuron and synapse models on the *Spikey* chip are different to the ones used in the original model, we have performed a behavioral fit in order to approximately reproduce the target firing patterns. Neuron and synapse parameters were first fitted in such a way as to generate clearly discernible attractors with relatively high average firing rates (see Figure 6D). Additional tuning was needed to compensate for missing neuronal adaptation, limitations in hardware configurability, parameter ranges and fixed-pattern noise affecting hardware parameters.

During hardware emulations, apart from the appearance of spontaneous attractors given only diffuse Poisson stimulation of the network (Figure 6C), we were able to observe two further interesting phenomena which are characteristic for the original attractor model.

When an attractor becomes active, its pyramidal cells enter a so-called UP state which is characterized by an elevated average membrane potential. Figure 6E clearly

shows the emergence of such UP-states on hardware. The onset of an attractor is characterized by a steep rise in pyramidal cell average membrane voltage, which then decays towards the end of the attractor due to synaptic short-term depression and/or competition from other attractors temporarily receiving stronger stimulation. On both flanks of an UP state, the average membrane voltage shows a slight undershoot, due to the inhibition by other active attractors.

A second important characteristic of cortical attractor models is their capability of performing *pattern completion* (Lundqvist et al., 2006). This means that a full pattern can be activated by stimulating only a subset of its constituent pyramidal cells (in the original model, by cells from cortical Layer 4, modeled by us as additional Poisson sources). The appearance of this phenomenon is similar to a phase transition from a resting state to a collective pyramidal UP-state occurring when a critical amount of pyramidal cells are stimulated. To demonstrate pattern completion, we have used the same setup as in the previous experiments, except for one pattern receiving additional stimulation. From an initial equilibrium between the three attractors (approximately equal active time), we have observed the expected sharp transition to a state where the stimulated attractor dominates the other two, occurring when one of its four minicolumns received L4 stimulus (Figure 6F).

The implementation of the attractor memory model is a particularly comprehensive showcase of the configurability and functionality of our neuromorphic platform due to the complexity of both model specifications and emergent dynamics. Starting from these results, the next-generation hardware (Schemmel et al., 2010) will be able to much more accurately model biological behavior, thanks to a more flexible, adapting neuron model and a significantly increased network size.

3.5. INSECT ANTENNAL LOBE MODEL

The high speedup factor of the *Spikey* chip makes it an attractive platform for neuromorphic data processing. Preprocessing of multivariate data is a common problem in signal and data analysis. In conventional computing, reduction of correlation between input channels is often the first step in the analysis of multidimensional data, achieved, e.g., by *principal component analysis* (PCA). The architecture of the olfactory system maps particularly well onto this problem (Schmuker & Schneider, 2007). We have implemented a network that is inspired by processing principles that have been described in the insect antennal lobe (AL), the first relay station from olfactory sensory neurons to higher brain areas. The function of the AL has been described to decorrelate the inputs from sensory neurons, potentially enabling more ef-

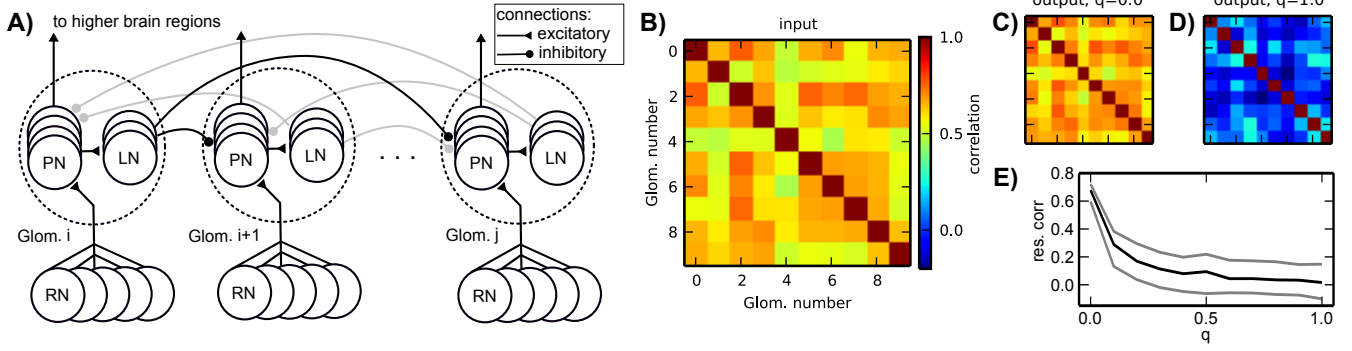


FIGURE 7: (A) Schematic of the insect antennal lobe network. Neuron populations are grouped in glomeruli (outlined by dotted lines), which exert lateral inhibition onto each other. RNs: receptor neurons (input), PNs: projection neurons (output), LNs: inhibitory local neurons. Some connections are grayed out to emphasize the connection principle. **(B)** Correlation matrix of the input data. **(C)** Correlation matrix of the output spike rates (PNs) without lateral inhibition, $q = 0.0$. **(D)** Correlation of the output with homogeneous lateral inhibition, $q = 1.0$. **(E)** Average pairwise correlation between glomeruli (median \pm 20th (black) and 80th (gray) percentile) in dependence of the overall strength of lateral inhibition q .

ficient memory formation and retrieval (Stopfer et al., 1997; Linster & Smith, 1997; Perez-Orive et al., 2004; Wilson & Laurent, 2005).

The availability of a network building block that achieves channel decorrelation is an important step toward high-performance neurocomputing. The aim of this experiment is to demonstrate that the previously studied rate-based AL model (Schmuker & Schneider, 2007) that reduces rate correlation between input channels is applicable to a spiking neuromorphic hardware system.

3.5.1. Network Topology

In the insect olfactory system, odors are first encoded into neuronal signals by receptor neurons (RNs) which are located on the antenna. RNs send their axons to the AL (Figure 7A). The AL is composed of glomeruli, spherical compartments where RNs project onto local inhibitory neurons (LNs) and projection neurons (PNs). LNs project onto other glomeruli, effecting lateral inhibition. PNs relay the information to higher brain areas where multimodal integration and memory formation takes place.

The architecture of our model reflects the neuronal connectivity in the insect AL (Figure 7A). RNs are modeled as spike train generators, which project onto the PNs in the corresponding glomerulus. The PNs project onto the LNs, which send inhibitory projections to the PNs in other glomeruli.

In biology, the AL network reduces the rate correlation between glomeruli, in order to improve stimulus separability and thus odor identification. Another effect of decorrelation is that the rate patterns encoding the stimuli become sparser, and use the available coding space more efficiently as redundancy is reduced. Our goal was

to demonstrate the reduction of rate correlations across glomeruli (*channel correlation*) by the AL-inspired spiking network. To this end, we generated patterns of firing rates with channel correlation. We created a surrogate data set exhibiting channel correlation using a copula, a technique that allows to generate correlated series of samples from an arbitrary random distribution and a covariance matrix (Nelsen, 1998). The covariance matrix was uniformly set to a target correlation of 0.6. Using this copula, we sampled 100 ten-dimensional data vectors from an exponential distribution. In the biological context, this is equivalent to having a repertoire of 100 odors, each encoded by ten receptors, and the firing rate of each input channel following a decaying exponential distribution. Values larger than e were clipped and the distribution was mapped to the interval $[0, 1]$ by applying $v = v/e$ for each value v . These values were then converted into firing rates between 20 and 55 spikes/s. The ten-dimensional data vector was presented to the network by mapping the ten firing rates onto the ten glomeruli, setting all single RNs in each glomerulus to fire at the respective target rates. Rates were converted to spike trains individually for each RN using the Gamma process with $\gamma = 5$. Each data vector was presented to the network for the duration of one second by making the RNs of each glomerulus fire with the specified rate. The inhibitory weights between glomeruli were uniform, i.e., all inhibitory connections shared the same weight. During one second of stimulus presentation, output rates were measured from PNs. One output rate per glomerulus was obtained by averaging the firing rate of all PNs in a glomerulus.

We have used 6 RN input streams per glomerulus, projecting in an all-to-all fashion onto 7 PNs, which in turn projected on 3 LNs per glomerulus.

3.5.2. Hardware Emulation

The purpose of the presented network was to reduce rate correlation between input channels. As in other models, fixed-pattern noise across neurons had a detrimental effect on the function of the network. We exploited the specific structure of our network to implement more efficient calibration than can be provided by standard calibration methods (Section 2.4). Our calibration algorithm targeted PNs and LNs in the first layer of the network. During calibration, we turned off all projections between glomeruli. Its aim was to achieve a homogeneous response across PNs and LNs respectively, i.e., within $\pm 10\%$ of a target rate. The target rate was chosen from the median response rate of uncalibrated neurons. For neurons whose response rate was too high it was sufficient to reduce the synaptic weight of the excitatory input from RNs. For those neurons with a too low rate the input strength had to be increased. The excitatory synaptic weight of the input from RNs was initially already at its maximum value and could not be increased. As a workaround we used PNs from the same glomerulus to add additional excitatory input to those “weak” neurons. We ensured that no recurrent excitatory loops were introduced by this procedure. If all neurons in a glomerulus were too weak, we recruit another external input stream to achieve the desired target rate. Once the PNs were successfully calibrated (less than 10% deviation from the target rate), we used the same approach to calibrate the LNs in each glomerulus.

To assess the performance of the network we have compared the channel correlation in the input and in the output. The channel correlation matrix \mathbf{C} was computed according to

$$C_{i,j} = d^{\text{Pearson}}(\boldsymbol{\nu}_{\text{glom},i}, \boldsymbol{\nu}_{\text{glom},j}), \quad (5)$$

with $d^{\text{Pearson}}(\cdot, \cdot)$ the Pearson correlation coefficient between two vectors. For the input correlation matrix $\mathbf{C}^{\text{input}}$, the vector $\boldsymbol{\nu}_{\text{glom},i}$ contained the average firing rates of the six RNs projecting to the i th glomerulus, with each element of this vector for one stimulus presentation. For the output correlation matrix $\mathbf{C}^{\text{output}}$ we used the rates from PNs instead of RNs. Thus, we obtained 10×10 matrices containing the rate correlations for each pair of input or output channels.

Figure 7B depicts the correlation matrix $\mathbf{C}^{\text{input}}$ for the input firing rates. When no lateral inhibition is present, $\mathbf{C}^{\text{input}}$ matches $\mathbf{C}^{\text{output}}$ (Figure 7C). We have systematically varied the strength of lateral inhibition by scaling all

inhibitory weights by a factor q , with $q = 0$ for zero lateral inhibition and $q = 1$ for inhibition set to its maximal strength. With increasing lateral inhibition, off-diagonal values in $\mathbf{C}^{\text{output}}$ approach zero and output channel correlation is virtually gone (Figure 7D). The amount of residual correlation to be present in the output can be controlled by adjusting the strength of lateral inhibition (Figure 7E).

Taken together, we demonstrated the implementation of an olfaction-inspired network to remove correlation between input channels on the *Spikey* chip. This network can serve as a preprocessing module for data analysis applications to be implemented on the *Spikey* chip. An interesting candidate for such an application is a spiking network for supervised classification, which may benefit strongly from reduced channel correlations for faster learning and better discrimination (Häusler et al., 2011).

3.6. LIQUID STATE MACHINE

Liquid state machines (LSMs) as proposed by Maass et al. (2002) and Jaeger (2001) provide a generic framework for computation on continuous input streams. The *liquid*, a recurrent network, projects an input into a high-dimensional space which is subsequently read out. It has been proven that LSMs have universal computational power for computations with fading memory on functions of time (Maass et al., 2002). In the following, we show that classification performance of a LSM emulated on our hardware is comparable to the corresponding computer simulation. Learning the synaptic weights iteratively on-chip inherently compensates for fixed-pattern noise. A trained system can then be used as an autonomous, fast and low-power spiking classifier.

3.6.1. Network Topology

The LSM consists of two major components: the recurrent liquid network itself and a spike-based classifier. A general purpose liquid needs to meet the separation property (Maass et al., 2002), which requires that different inputs are mapped to different outputs, for a wide range of possible inputs. Therefore, we use a network topology similar to the one proposed by Bill et al. (2010) (Figure 8). It consists of an excitatory and inhibitory population both having recurrent as well as feedforward connections.

The readout is realized by means of a tempotron (Gütig & Sompolinsky, 2006), which is compatible with our hardware due to its spike-based nature. Furthermore, its modest single neuron implementation leaves most hardware resources to the liquid. The afferent synaptic weights are trained with the method described in Gütig & Sompolinsky (2006), which effectively implements gradient descent dynamics. Upon training, the tempotron distinguishes

between two input classes by emitting either one or no spike within a certain time window. The former is artificially enforced by blocking all further incoming spikes after the first spike occurrence.

The PSP kernel of a LIF neuron with current-based synapses is given by

$$K(t - t_i) = A \left(e^{-\frac{t-t_i}{\tau_m}} - e^{-\frac{t-t_i}{\tau_s}} \right) \cdot \Theta(t - t_i), \quad (6)$$

with the membrane time constant τ_m and the synaptic time constant τ_s , respectively. Here, A denotes a constant PSP scaling factor, t_i the time of the i th incoming spike and $\Theta(t)$ the Heaviside step function.

During learning, weights are updated as follows

$$\Delta w_j^n = \begin{cases} 0 & \text{correct} \\ \alpha(n) \sum_{t_{i,j} < t_{\max}} K(t_{\max} - t_{i,j}) & \text{erroneous,} \end{cases} \quad (7)$$

where Δw_j^n is the weight update corresponding to the j th afferent neuron after the n th learning iteration with learning rate $\alpha(n)$. The spike time of the tempotron, or otherwise the time of highest membrane potential, is denoted with t_{\max} . In other words, for trials where an erroneous spike was elicited, the excitatory afferents with a causal contribution to this spike are weakened and inhibitory ones are strengthened according to Equation 7. In case the tempotron did not spike even though it should have, the weights are modulated the other way round, i.e. excitatory weights are strengthened and inhibitory ones are weakened. This learning rule has been implemented on hardware with small modifications, due to the conductance-based nature of the hardware synapses (see below).

The tempotron is a binary classifier, hence any task needs to be mapped to a set of binary decisions. Here, we have chosen a simple binary task to evaluate the performance of the LSM. The challenge was to distinguish spike train segments in a continuous data stream composed of two templates with identical rates. In order to generate the input, we cut two long template spike trains into segments of 50 ms each. For any cut we then randomly picked the corresponding spike segment from the one or the other template, successively composing new spike sequences. Additionally, Gaussian noise with a standard deviation of $\sigma = 1$ ms was added to each spike time. The samples were then streamed into the liquid one at a time. Tempotrons were trained to identify the origin of a certain segment, within the final 50 ms given the liquid activity as input. Not only did this task allow to determine the classification capabilities of the LSM, but it also put the liquid's fading memory to the test: classification becomes increasingly difficult, the further back in time the inter-

esting segment lies. It can be assumed that the memory is mostly contributed by transient liquid activity rather than the tempotron, since all its time constants have been set far below 100 ms.

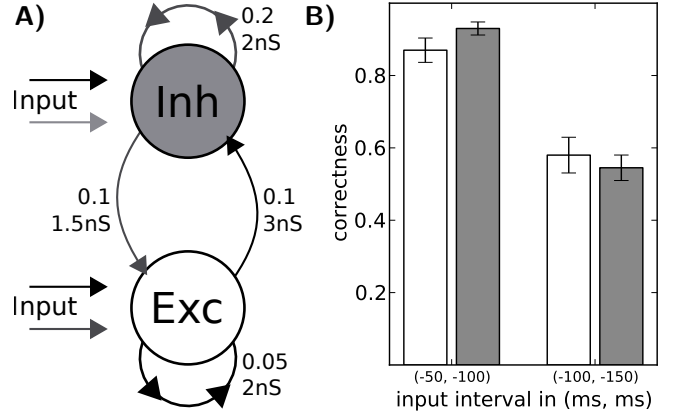


FIGURE 8: (A) Network architecture of the liquid network with up to 191 neurons, leaving at least one neuron for the tempotron. The ratio of excitatory to inhibitory neurons is 80:20. Each neuron receives 4 inputs from a pool of 32 excitatory and 32 inhibitory sources, respectively. **(B)** The LSM classification performance measured over 200 samples after 1000 training iterations for both hardware (white) and software (grey) implementation. Both implementations classify the input segment from 50 ms to 100 ms in the past with about 90% correctness. For inputs lying further behind in time, both implementations drop to chance level.

3.6.2. Hardware Emulation

The liquid itself does not impose any strong requirements on the hardware since virtually any network is suitable as long as the separation property is satisfied. We adapted a network from Bill et al. (2010) (Figure 8) which, in a similar form, had already been implemented on our hardware. However, STP was disabled, because at the time of the experiment it was not possible to exclusively enable STP for the liquid without severely affecting the performance of the tempotron.

The hardware implementation of the tempotron required more attention, since only conductance-based synapses are available. The dependence of spike efficacies on the actual membrane potential was neglected, because the rest potential was chosen to be close to the firing threshold, with the reversal potentials far away. However, the asymmetric distance of excitatory and inhibitory reversal potentials from the sub-threshold regime needed compensation. This was achieved by scaling all excitatory weights by $(\bar{V}_m - E_{\text{inh}})/(\bar{V}_m - E_{\text{exc}})$, where \bar{V}_m corresponds to the mean neuron membrane voltage and $E_{\text{exc}}/E_{\text{inh}}$ is the excitatory/inhibitory reversal po-

tentials. Discontinuities in spike efficacies for synapses changing from excitatory to inhibitory or vice versa were avoided by prohibiting such transitions. Finally, membrane potential shunting after the first spike occurrence is neither possible on our hardware nor very biological and had therefore been neglected, as already proposed by Gütig & Sompolinsky (2006).

Even though the tempotron was robust against fixed-pattern noise due to on-chip learning, the liquid required modifications. Therefore, firing thresholds were tuned independently in software and hardware to optimize the memory capacity and avoid violations of the separation property. Since hardware neurons share firing thresholds, the tempotron was affected accordingly (see Table 1). Additionally, the learning curve $\alpha(n)$ was chosen individually for software and hardware due to the limited resolution of synaptic weights on the latter.

The results for software and hardware implementations are illustrated in Figure 8. Both LSMs performed at around 90% classification correctness for the spiketrain segment that lied 50 ms to 100 ms in the past with respect to the end of the stimulus. For inputs lying even further away in time, performances dropped to chance level (50% for a binary task), independent of the simulation back-end.

Regarding the classification capabilities of the LSM, our current implementation allows a large variety of tasks to be performed. Currently, e.g., we are working on handwritten digit recognition with the very same setup on the *Spikey* chip. Even without a liquid, our implementation of the tempotron (or populations thereof) makes an excellent neuromorphic classifier, given its bandwidth-friendly sparse response and robustness against fixed-pattern noise.

4. DISCUSSION

We have successfully implemented a variety of neural microcircuits on a single universal neuromorphic substrate. The observed activity patterns are equivalent to those obtained by software simulations. In particular, the emulations benefit from the inherent advantages of a neuromorphic implementation, namely low power consumption and accelerated operation compared to software simulation on conventional von-Neumann machines. Previous accounts of networks implemented on the *Spikey* system include computing with high-conductance states (Kaplan et al., 2009), or self-stabilizing recurrent networks (Bill et al., 2010).

In this contribution, we have presented a number of new networks and extensions of previous implementations. Our synfire chain implementation achieves reliable signal propagation over years of biological time from one single stimulation, while synchronizing and filtering these signals (Section 3.1). Our extension of the network from

Bill et al. (2010) to exhibit asynchronous irregular firing behavior is an important achievement in the context of reproducing stochastic activity patterns found in cortex (Section 3.2). We have realized winner-take-all networks on our hardware system (Section 3.3), which are essential building blocks for many cortical models involving some kind of attractor states (e.g., the decision-making model by Soltani & Wang, 2010). The emulated cortical attractor model provides an implementation of working memory for computation with cortical columns (Section 3.4). Additionally, we have used the *Spikey* system for preprocessing of multivariate data inspired by biological archetypes (Section 3.5) and machine learning (Section 3.6). Most of these networks allocate the full number of neurons receiving input from one synapse array on the *Spikey* chip, but with different sets of neuron and synapse parameters and especially vastly different connectivity patterns, thereby emphasizing the remarkable configurability of our neuromorphic substrate.

However, the translation of such models requires modifications to allow execution on our hardware. The most prominent cause for such modifications is fixed-pattern noise across analog hardware neurons and synapses. In most cases, especially when population rate coding is involved, it is sufficient to compensate for this variability by averaging spiking activity over many neurons. For the data decorrelation and machine learning models, we have additionally trained the synaptic weights on the chip to achieve finer equilibration of the variability at critical network nodes. Especially when massive downscaling is required in order for models to fit onto the substrate, fixed pattern noise presents an additional challenge because the same amount of information needs to be encoded by fewer units. For this reason, the implementation of the cortical attractor memory network required additional heuristic activity fitting procedures.

The usability of the *Spikey* system, especially for neuroscientists with no neuromorphic engineering background, is provided by an integrated development environment that allows efficient use of the system without knowledge about the intricate details of the hardware implementation (Brüderle et al., 2010; Schmuker et al., 2011). Networks can be developed using the PyNN metalanguage and optionally be prototyped on software simulators before running on the *Spikey* system (Davison et al., 2009; Brüderle & Müller et al., 2009). This rather easy configuration and operation of the *Spikey* chip allows the implementation of many other neural network models.

There exist also boundaries to the universal applicability of our hardware system. One limitation inherent to this type of neuromorphic device is the choice of implemented models for neuron and synapse dynamics. Models requiring, e.g., neuronal adaptation or exotic synaptic

plasticity rules are difficult, if not impossible to be emulated on this substrate. Also, the total number of neurons and synapses set a hard upper bound on the size of networks that can be emulated. However, the next generation of our highly accelerated hardware system will increase the number of available neurons and synapses by a factor of 10^3 , and provide extended configurability for each of these units (Schemmel et al., 2010).

The main purpose of our hardware system is to provide a flexible platform for highly accelerated emulation of spiking neuronal networks. Other research groups pursue different design goals for their hardware systems. Some focus on dedicated hardware providing specific network topologies (e.g., Merolla & Boahen, 2006; Chicca et al., 2007), or comprising few neurons with more complex dynamics (e.g., Chen et al., 2010; Grassia et al., 2011). Others develop hardware systems of comparable configurability, but operate in biological real-time, mostly using off-chip communication (Vogelstein et al., 2007; Imam et al., 2012; Choudhary et al., 2012). Purely digital systems (Merolla et al., 2011) and field-programmable analog arrays (FPAA; Basu et al., 2010) provide even more flexibility in configuration than our system, but have much smaller speed-up factors.

With the ultimate goal of brain size emulations, there exists a clear requirement for increasing the size and complexity of neuromorphic substrates. An accompanying upscaling of the fitting and calibration procedures presented here appears impractical for such orders of magnitude and can only be done for a small subset of components. Rather, it will be essential to step beyond simulation equivalence as a quality criterion for neuromorphic computing, and to develop a theoretical framework for circuits that are robust against, or even exploit the inherent imperfections of the substrate for achieving the required computational functions.

ACKNOWLEDGMENTS

We would like to thank Dan Husmann, Stefan Philipp, Bernhard Kaplan, and Moritz Schilling for their essential contributions to the neuromorphic platform, Johannes Bill, Jens Kremkow, Anders Lansner, Mikael Lundqvist and Emre Neftci for assisting with the hardware implementation of the network models, Oliver Breitwieser for data analysis and Venelin Petkov for characterisation measurements of the *Spikey* chip.

The research leading to these results has received funding by the European Union 6th and 7th Framework Programme under grant agreement no. 15879 (FACETS), no. 269921 (BrainScaleS) and no. 243914 (Brain-i-Nets). Michael Schmuken has received support from the German ministry for research and education (BMBF) to Bernstein Center for Computational Neuroscience Berlin (grant no.

01GQ1001D) and from Deutsche Forschungsgemeinschaft within SPP 1392 (grant no. SCHM 2474/1-1).

The main contributors for each section are denoted with author initials: neuromorphic system (AG & EM); synfire chain (PM); balanced random network (TP); winner-take-all network (TP); cortical attractor model (MP); antennal lobe model (MS); liquid state machine (SJ). All authors contributed to writing this paper.

REFERENCES

- Abeles, M., Hayon, G., & Lehmann, D. (2004). Modeling compositionality by dynamic binding of synfire chains. *J. Comput. Neurosci.* 17(2), 179–201.
- Aertsen, A., Diesmann, M., & Gewaltig, M.-O. (1996). Propagation of synchronous spiking activity in feedforward neural networks. *J. Physiol. (Paris)* 90(3/4), 243–247.
- Akay, M. (2007). *Handbook of neural engineering - Part II: Neuro-nanotechnology: Artificial implants and neural prosthesis*. Wiley-IEEE Press.
- Aviel, Y., Mehring, C., Abeles, M., & Horn, D. (2003). On embedding synfire chains in a balanced network. *Neural Comput.* 15(6), 1321–1340.
- Baker, S. N., Spinks, R., Jackson, A., & Lemon, R. N. (2001). Synchronization in monkey motor cortex during a precision grip task. I. Task-dependent modulation in single-unit synchrony. *J. Neurophysiol.* 85(2), 869–85.
- Basu, A., Ramakrishnan, S., Petre, C., Koziol, S., Brink, S., & Hasler, P. (2010). Neural dynamics in reconfigurable silicon. *IEEE Trans. Biomed. Circuits Syst.* 4(5), 311–319.
- Bi, G., & Poo, M. (1998). Synaptic modifications in cultured hippocampal neurons: Dependence on spike timing, synaptic strength, and postsynaptic cell type. *J. Neurosci.* 18, 10464–10472.
- Bill, J., Schuch, K., Brüderle, D., Schemmel, J., Maass, W., & Meier, K. (2010). Compensating inhomogeneities of neuromorphic VLSI devices via short-term synaptic plasticity. *Front. Comput. Neurosci.* 4(129).
- Brüderle, D., Bill, J., Kaplan, B., Kremkow, J., Meier, K., Müller, E., & Schemmel, J. (2010). Simulator-like exploration of cortical network architectures with a mixed-signal VLSI system. In *Proceedings of the 2010 International Symposium on Circuits and Systems (ISCAS)*. IEEE Press.
- Brüderle, D., Müller, E., Davison, A., Müller, E., Schemmel, J., & Meier, K. (2009). Establishing a novel modeling tool: A python-based interface for a neuromorphic hardware system. *Fed. Proc.* 3(17).
- Brüderle, D., Petrovici, M., Vogginger, B., Ehrlich, M., Pfeil, T., Millner, S., Grübl, A., Wendt, K., Müller, E., Schwartz, M.-O., Husmann de Oliveira, D., Jeltsch, S., Fieres, J., Schilling, M., Müller, P., Breitwieser, O., Petkov, V., Müller, L., Davison, A. P., Krishnamurthy, P., Kremkow,

- J., Lundqvist, M., Muller, E., Partzsch, J., Scholze, S., Zühl, L., Destexhe, A., Diesmann, M., Potjans, T. C., Lansner, A., Schüffny, R., Schemmel, J., & Meier, K. (2011). A comprehensive workflow for general-purpose neural modeling with highly configurable neuromorphic hardware systems. *Biol. Cybern.* 104, 263–296.
- Brunel, N. (2000). Dynamics of sparsely connected networks of excitatory and inhibitory spiking neurons. *J. Comput. Neurosci.* 8(3), 183–208.
- Carnevale, T., & Hines, M. (2006). *The NEURON Book*. Cambridge: Cambridge University Press.
- Chen, H., Saïghi, S., Buhry, L., & Renaud, S. (2010). Real-time simulation of biologically realistic stochastic neurons in VLSI. *IEEE Trans. Neural Netw.* 21(9), 1511–1517.
- Chicca, E., Whatley, A. M., Lichtsteiner, P., Dante, V., Delbruck, T., Del Giudice, P., Douglas, R. J., & Indiveri, G. (2007). A multichip pulse-based neuromorphic infrastructure and its application to a model of orientation selectivity. *IEEE Trans. Circuits Syst. I, Reg. Papers* 54(5), 981–993.
- Choudhary, S., Sloan, S., Fok, S., Neckar, A., Trautmann, E., Gao, P., Stewart, T., Elias Smith, C., & Boahen, K. (2012). Silicon neurons that compute. In A. Villa, W. Duch, P. Erdi, F. Masulli, & G. Palm (Eds.), *Artificial Neural Networks and Machine Learning – ICANN 2012*, Volume 7552 of *Lecture Notes in Computer Science*, pp. 121–128. Springer Berlin / Heidelberg.
- Davison, A., Brüderle, D., Eppler, J. M., Kremkow, J., Muller, E., Pecevski, D., Perrinet, L., & Yger, P. (2009). PyNN: a common interface for neuronal network simulators. *Front. Neuroinformatics* 2(11).
- Davison, A., Muller, E., Brüderle, D., & Kremkow, J. (2010). A common language for neuronal networks in software and hardware. *The Neuromorphic Engineer*.
- Dayan, P., & Abbott, L. F. (2001). *Theoretical Neuroscience*. Cambridge: MIT Press.
- Diesmann, M., Gewaltig, M.-O., & Aertsen, A. (1999). Stable propagation of synchronous spiking in cortical neural networks. *Nature* 402(6761), 529–533.
- Eppler, J. M., Helias, M., Muller, E., Diesmann, M., & Gewaltig, M. (2009). PyNEST: a convenient interface to the NEST simulator. *Front. Neuroinformatics* 2, 12.
- Fieres, J. and. Grübl, A., Philipp, S., Meier, K., Schemmel, J., & Schürmann, F. (2004). A platform for parallel operation of VLSI neural networks. In *Proceedings of the 2004 Brain Inspired Cognitive Systems Conference (BICS)*, University of Stirling, Scotland, UK.
- Gewaltig, M.-O., & Diesmann, M. (2007). NEST (NEural Simulation Tool). *Scholarpedia* 2(4), 1430.
- Grassia, F., Buhry, L., Lévi, T., Tomas, J., Destexhe, A., & Saïghi, S. (2011). Tunable neuromimetic integrated system for emulating cortical neuron models. *Front. Neurosci.* 5(134).
- Grossberg, S. (1973). Contour enhancement, short term memory, and constancies in reverberating neural networks. *Stud. Appl. Math.* 52(3), 213–257.
- Gupta, A., Wang, Y., & Markram, H. (2000). Organizing principles for a diversity of GABAergic interneurons and synapses in the neocortex. *Science* 287, 273–278.
- Gütig, R., & Sompolinsky, H. (2006). The tempotron: a neuron that learns spike timing-based decisions. *Nat. Neurosci.* 9(3), 420–428.
- Häusler, C., Nawrot, M. P., & Schmuker, M. (2011). A spiking neuron classifier network with a deep architecture inspired by the olfactory system of the honeybee. In *2011 5th International IEEE/EMBS Conference on Neural Engineering*, pp. 198–202. IEEE Press.
- Hines, M., Davison, A. P., & Muller, E. (2009). Neuron and python. *Front. Neuroinformatics* 3.
- Imam, N., Cleland, T. A., Manohar, R., Merolla, P. A., Arthur, J. V., Akopyan, F., & Modha, D. S. (2012). Implementation of olfactory bulb glomerular layer computations in a digital neurosynaptic core. *Front. Neurosci.* 6(83).
- Indiveri, G., Chicca, E., & Douglas, R. (2006). A VLSI array of low-power spiking neurons and bistable synapses with spike-timing dependent plasticity. *IEEE Trans. Neural Netw.* 17(1), 211–221.
- Indiveri, G., Chicca, E., & Douglas, R. (2009). Artificial cognitive systems: From VLSI networks of spiking neurons to neuromorphic cognition. *Cognitive Computation* 1(2), 119–127.
- Itti, L., & Koch, C. (2001). Computational modeling of visual attention. *Nat. Rev. Neurosci.* 2(3), 194–203.
- Jaeger, H. (2001). The “echo state” approach to analysing and training recurrent neural networks. Technical Report GMD Report 148, German National Research Center for Information Technology.
- Kaplan, B., Brüderle, D., Schemmel, J., & Meier, K. (2009). High-conductance states on a neuromorphic hardware system. In *Proceedings of the 2009 International Joint Conference on Neural Networks (IJCNN)*, Atlanta, pp. 1524–1530.
- Kremkow, J., Aertsen, A., & Kumar, A. (2010). Gating of signal propagation in spiking neural networks by balanced and correlated excitation and inhibition. *J. Neurosci.* 30(47), 15760–15768.
- Kremkow, J., Perrinet, L. U., Masson, G. S., & Aertsen, A. (2010). Functional consequences of correlated excitatory and inhibitory conductances in cortical networks. *J. Comput. Neurosci.* 28(3), 579–594.

- Kumar, A., Schrader, S., Aertsen, A., & Rotter, S. (2008). The high-conductance state of cortical networks. *Neural Comput.* 20(1), 1–43.
- Lazzaro, J., Ryckebusch, S., Mahowald, M., & Mead, C. (1988). Winner-take-all networks of $o(n)$ complexity. In *Advances in Neural Information Processing Systems (NIPS)*, Denver, pp. 703–711.
- Linster, C., & Smith, B. H. (1997). A computational model of the response of honey bee antennal lobe circuitry to odor mixtures: overshadowing, blocking and unblocking can arise from lateral inhibition. *Behav. Brain. Res.* 87, 1–14.
- Litvak, V., Sompolinsky, H., Segev, I., & Abeles, M. (2003). On the transmission of rate code in long feed-forward networks with excitatory-inhibitory balance. *J. Neurosci.* 23(7), 3006–3015.
- Lundqvist, M., Compte, A., & Lansner, A. (2010). Bistable, irregular firing and population oscillations in a modular attractor memory network. *PLoS Comput. Biol.* 6(6), e1000803.
- Lundqvist, M., Rehn, M., Djurfeldt, M., & Lansner, A. (2006). Attractor dynamics in a modular network model of neocortex. *Network: Comput. Neural Systems* 17(3), 253–276.
- Maass, W. (2000). On the computational power of winner-take-all. *Neural Comput.* 12(11), 2519–2535.
- Maass, W., Natschläger, T., & Markram, H. (2002). Real-time computing without stable states: a new framework for neural computation based on perturbation. *Neural Comput.* 14(11), 2531–2560.
- Marder, E., & Goaillard, J.-M. (2006). Variability, compensation and homeostasis in neuron and network function. *Nat. Rev. Neurosci.* 7(7), 563–574.
- Markram, H., Wang, Y., & Tsodyks, M. (1998). Differential signaling via the same axon of neocortical pyramidal neurons. *Proc. Natl. Acad. Sci. USA* 95(9), 5323–5328.
- Mead, C. (1989). *Analog VLSI and neural systems*. Boston, MA, USA: Addison-Wesley.
- Merolla, P., Arthur, J., Akopyan, F., Imam, N., Manohar, R., & Modha, D. (2011). A digital neurosynaptic core using embedded crossbar memory with 45pJ per spike in 45nm. In *Proceedings of the 2011 Custom Integrated Circuits Conference (CICC)*, pp. 1–4. IEEE Press.
- Merolla, P., & Boahen, K. (2006). Dynamic computation in a recurrent network of heterogeneous silicon neurons. In *Proceedings of the 2006 International Symposium on Circuits and Systems (ISCAS)*, Island of Kos, pp. 4539–4542. IEEE Press.
- Neftci, E., & Indiveri, G. (2010). A device mismatch compensation method for VLSI neural networks. In *Proceedings of the 2010 Biomedical Circuits and Systems Conference (BioCAS)*, pp. 262–265. IEEE Press.
- Nelsen, R. B. (1998). *An Introduction to Copulas (Lecture Notes in Statistics)* (1 ed.). Springer.
- Oster, M., Douglas, R., & Liu, S. (2009). Computation with spikes in a winner-take-all network. *Neural Comput.* 21(9), 2437–2465.
- Perez-Orive, J., Bazhenov, M., & Laurent, G. (2004). Intrinsic and circuit properties favor coincidence detection for decoding oscillatory input. *J. Neurosci.* 24(26), 6037–47.
- Perkel, D. H., Gerstein, G. L., & Moore, G. P. (1967). Neuronal spike trains and stochastic point processes. II. Simultaneous spike trains. *Biophys. J.* 7(4), 419–440.
- Pfeil, T., Potjans, T. C., Schrader, S., Potjans, W., Schemmel, J., Diesmann, M., & Meier, K. (2012). Is a 4-bit synaptic weight resolution enough? - constraints on enabling spike-timing dependent plasticity in neuromorphic hardware. *Front. Neurosci.* 6(90).
- Prut, Y., Vaadia, E., Bergman, H., Haalman, I., Hamutal, S., & Abeles, M. (1998). Spatiotemporal structure of cortical activity: Properties and behavioral relevance. *J. Neurophysiol.* 79(6), 2857–2874.
- Renaud, S., Tomas, J., Lewis, N., Bornat, Y., Daouzli, A., Rudolph, M., Destexhe, A., & Saïghi, S. (2010). PAX: A mixed hardware/software simulation platform for spiking neural networks. *Neural Networks* 23(7), 905–916.
- Rolls, E. T., & Deco, G. (2010). *The Noisy Brain: Stochastic Dynamics as a Principle*. Oxford University Press.
- Schemmel, J., Brüderle, D., Grünbl, A., Hock, M., Meier, K., & Millner, S. (2010). A wafer-scale neuromorphic hardware system for large-scale neural modeling. In *Proceedings of the 2010 International Symposium on Circuits and Systems (ISCAS)*, Paris, pp. 1947–1950. IEEE Press.
- Schemmel, J., Brüderle, D., Meier, K., & Ostendorf, B. (2007). Modeling synaptic plasticity within networks of highly accelerated I&F neurons. In *Proceedings of the 2007 International Symposium on Circuits and Systems (ISCAS)*, New Orleans. IEEE Press.
- Schemmel, J., Grünbl, A., Meier, K., & Müller, E. (2006). Implementing synaptic plasticity in a VLSI spiking neural network model. In *Proceedings of the 2006 International Joint Conference on Neural Networks (IJCNN)*, Vancouver, pp. 1–6. IEEE Press.
- Schmuker, M., Brüderle, D., Schrader, S., & Nawrot, M. P. (2011). Ten thousand times faster: Classifying multidimensional data on a spiking neuromorphic hardware system. *Front. Comput. Neurosci. Conference Abstract: BC11: Computational Neuroscience & Neurotechnology Bernstein Conference & Neurax Annual Meeting 2011*(109).
- Schmuker, M., & Schneider, G. (2007). Processing and classification of chemical data inspired by insect olfaction. *Proc. Natl. Acad. Sci. USA* 104(51), 20285–20289.

- Schrader, S., Diesmann, M., & Morrison, A. (2010). A compositionality machine realized by a hierarchic architecture of synfire chains. *Front. Comput. Neurosci.* 4, 154.
- Schrader, S., Grün, S., Diesmann, M., & Gerstein, G. (2008). Detecting synfire chain activity using massively parallel spike train recording. *J. Neurophysiol.* 100, 2165–2176.
- Serrano-Gotarredona, R., Oster, M., Lichtsteiner, P., Linares-Barranco, A., Paz-Vicente, R., Gómez-Rodríguez, F., Kolle Riis, H., Delbrück, T., Liu, S.-C., Zahnd, S., Whatley, A. M., Douglas, R., Häfliger, P., Jimenez-Moreno, G., Civit, A., Serrano-Gotarredona, T., Acosta-Jiménez, A., & Linares-Barranco, B. (2006). AER building blocks for multi-layer multi-chip neuromorphic vision systems. In Y. Weiss, B. Schölkopf, & J. Platt (Eds.), *Adv. Neural. Inf. Process. Syst.*, pp. 1217–1224. Cambridge, MA: MIT Press.
- Soltani, A., & Wang, X.-J. (2010). Synaptic computation underlying probabilistic inference. *Nat. Neurosci.* 13(1), 112–9.
- Song, S., Miller, K. D., & Abbott, L. F. (2000). Competitive Hebbian learning through spike-timing-dependent synaptic plasticity. *Nat. Neurosci.* 3(9), 919–926.
- Stopfer, M., Bhagavan, S., Smith, B. H., & Laurent, G. (1997). Impaired odour discrimination on desynchronization of odour-encoding neural assemblies. *Nature* 390(6655), 70–4.
- Tetzlaff, T., Morrison, A., Timme, M., & Diesmann, M. (2005). Heterogeneity breaks global synchrony in large networks. In *Proceedings of the 30th Göttingen Neurobiology Conference*.
- Tsodyks, M. V., & Markram, H. (1997). The neural code between neocortical pyramidal neurons depends on neurotransmitter release probability. *Proc. Natl. Acad. Sci. USA* 94, 719–723.
- van Vreeswijk, C., & Sompolinsky, H. (1996). Chaos in neuronal networks with balanced excitatory and inhibitory activity. *Science* 274, 1724–1726.
- Vogels, T. P., & Abbott, L. F. (2005). Signal propagation and logic gating in networks of integrate-and-fire neurons. *J. Neurosci.* 25(46), 10786–10795.
- Vogelstein, R., Mallik, U., Vogelstein, J., & Cauwenberghs, G. (2007). Dynamically reconfigurable silicon array of spiking neurons with conductance-based synapses. *IEEE Trans. Neural Netw.* 18(1), 253–265.
- Wilson, R. I., & Laurent, G. (2005). Role of GABAergic inhibition in shaping odor-evoked spatiotemporal patterns in the drosophila antennal lobe. *J. Neurosci.* 25(40), 9069–9079.
- Yazdanbakhsh, A., Babadi, B., Rouhani, S., Arabzadeh, E., & Abbassian, A. (2002). New attractor states for synchronous activity in synfire chains with excitatory and inhibitory coupling. *Biol. Cybern.* 86, 367–378.